Organic & Biomolecular Chemistry

ROYAL SOCIETY OF CHEMISTRY

PAPER

View Article Online
View Journal | View Issue

Cite this: *Org. Biomol. Chem.*, 2020, **18**, 6935

Carbazole modified oligonucleotides: synthesis, hybridization studies and fluorescence properties†

Alaa S. Gouda, ‡[a,b] Łukasz Przypis, ‡[c] Krzysztof Walczak, [c] Per T. Jørgensen [a] and Jesper Wengel *[a]

Received 28th July 2020,
Accepted 21st August 2020

DOI: 10.1039/d0ob01553a

rsc.li/obc

Synthesis of the novel thiophenyl carbazole phosphoramidite DNA building block **5** was accomplished in four steps using a Suzuki–Miyaura cross-coupling reaction from the core carbazole and it was seamlessly accommodated into a 9-mer DNA-based oligonucleotide by incorporation at the flanking 5′-end in combination with a central insertion of an LNA-T nucleotide. The carbazole-containing oligonucleotide was combined in different duplex hybrids, which were characterized by thermal denaturation, circular dichroism and fluorescence studies. The carbazole monomer modulates the duplex stability in various ways. Thus, monomer **Z** increased the thermal stability of the 9-mer towards the complementary 9-mer/15-mer DNA duplex by 4.2 °C. Furthermore, indications of its intercalation into the duplex were obtained by modeling studies and robust decreases in fluorescence emission intensities upon duplex formation. In contrast, no clear intercalating tendency was corroborated for monomer **Z** within the DNA/RNA hybrid duplex as indicated by moderate quenching of the fluorescence and similar duplex thermal stabilities relative to the corresponding control duplex. The recognition efficiencies of the carbazole modified oligonucleotide toward single nucleotide mismatches were studied with two 15-mer model targets (DNA and RNA). For both systems, mismatches positioned at the juxtaposition of the carbazole monomer showed pronounced deceases in thermal denaturation temperature. Steady-state fluorescence emission studies of all mismatched duplexes with incorporation of **Z** monomer typically displayed efficient fluorescence quenching.

Introduction

Over the last two decades, research in the field of synthetic nucleic acids has sparked a plethora of biologically relevant applications.[1–5] Previous studies reported that oligonucleotide (ON) analogues inducing high duplex stability and sequence specificity towards target DNA or RNA single strands are interesting as therapeutics or diagnostics.[6] To date, a diverse assortment of modified ONs have been prepared by solid-phase DNA synthesis using chemically modified nucleosides and non-nucleosidic building blocks with the aim of optimizing *e.g.* binding affinity, mismatch discrimination, spectroscopic properties and *in vivo* stability.[7–11]

One nucleotide modification also used in this study is locked nucleic acids (LNA) with a conformationally locked C3′-*endo* (North-type) furanose ring thus mimicking RNA nucleotides.[12,13] Incorporation of one or more LNA monomers into ONs has been shown to induce excellent hybridization properties, especially towards complementary single-stranded RNA.[14]

A variety of fluorescent probes have been inserted into ONs with the purpose of specific and sensitive detection of hybridization towards complementary DNA/RNA. This can be achieved by observing the changes of fluorescence, through enhanced or quenched emission upon duplex formation.[15–20]

Fluorescent probes comprising polyaromatic compounds have been intensively studied to label DNA for biochemical and biological applications. Typical labels of this class include pyrene,[21] perylene,[22] and phenanthroline[23] known to possibly form non-covalent π-stacking interactions and/or intercalation with nucleic acids[24–27] or with other polyaromatic compounds.[28–34]

Carbazole and its derivatives which in general have interesting spectral and electronic properties were found to integrate well in DNA without compromising the hybrid stability. Thus, it has been reported that carbazole monomers are known to modulate G-quadruplexes and duplexes.[35–38] In addition, car-

[a]*Biomolecular Nanoscale Engineering Center, Department of Physics, Chemistry and Pharmacy, University of Southern Denmark, Campusvej 55, 5230 Odense M, Denmark. E-mail: jwe@sdu.dk; Tel: +45 65502510*
[b]*Department of Chemistry, Faculty of Science, Benha University, Benha13518, Egypt*
[c]*Department of Organic Chemistry, Biochemistry and Biotechnology, Silesian University of Technology, Poland*

†Electronic supplementary information (ESI) available: ^{1}H-,^{13}C-NMR, ^{31}P-NMR, HSQC, HMBC, H-HCOSY and HRMS of the synthesized compounds **2–5** (Fig. S1–S16). The IE-HPLC trace and MALDI-TOF mass spectrometry data of oligonucleotides (**ON1–ON3**). The representative UV melting absorption curves, first derivatives curves and CD spectral analysis for all DNA/DNA and DNA/RNA duplexes are shown in Fig. S17–S27. See DOI: 10.1039/d0ob01553a

‡These authors contributed equally to this work.

bazole nucleotide monomers have been reported to induce elevated duplex stability as a result of increased stacking interactions involving the extended aromatic structure.[38] Furthermore, 3-cyanovinylcarbazole-modified ONs with the threoninol linker showed promising DNA photo-cross-linking reactivity,[39] and specific and reversible photochemical labeling of single- and double-stranded plasmid DNA.[40]

Taking into account the general sensitivity of carbazole-functionalized probes toward hybridization,[36–38] and the high-affinity hybridization of LNA-T,[14,41–45] we present here a new ON design that combines the interesting fluorescence properties of the thiophenyl-substituted carbazole (absorbs around 310 nm and emits around 400 nm) together with the known stabilization properties of the LNA-T monomer. We choose to incorporate one LNA-T monomer into the middle of the 9-mer DNA ON due to the known positive effect of LNA on the duplex thermostability, favorable mismatch discrimination and improved resistance toward nucleolytic digestion.[45] We also investigate the impact on the intercalating properties when placing a bulky 3-thiophenyl-substituted carbazole probe at the 5′-end of a 9-mer DNA-type ON. Furthermore, we describe the synthesis of the thiophenyl carbazole phosphoramidite derivative **5**, its 5′-end incorporation into a 9-mer DNA-type ON, and its effects on binding affinity, mismatch discrimination and fluorescence emission properties (Fig. 1).

Results and discussion

Synthesis of the carbazole phosphoramidite building block

A synthetic route toward the thiophenyl carbazole phosphoramidite monomer **5** from the commercially available carbazole **1** was developed in four high yielding steps as shown in Scheme 1. The direct iodination reaction was performed on the carbazole core using mild conditions previously described by Przypis and Walczak,[46] *i.e.* using Barluenga's reagent (IPy_2BF_4) as an iodinating agent and copper sulphate in anhydrous acetonitrile under an atmosphere of nitrogen to afford 3-iodo-9*H*-carbazole (**2a**) as the major product in 79% yield. Purification of the 3-iodocarbazole **2a** was challenging when using chromatography. This is ascribed to the formation of a by-product tentatively assigned as the corresponding 3,6-diiodo-9*H*-carbazole according to TLC. However, it turned out to be possible to purify the product by recrystallization. *N*-Alkylation of 3-iodocarbazole **2a** was accomplished by treatment with 2-bromoethanol in the presence of potassium hydroxide in anhydrous dimethylformamide to furnish the corresponding *N*-hydroxyethylated 3-iodocarbazole **3** in 77% yield. An alternative synthetic methodology has been applied for synthesis of **3** from the carbazole precursor **1** by performing the above-mentioned two steps in a reverse order.[47] A thiophenyl moiety was introduced into the 3-position of the iodocarbazole alcohol **3** by means of a Suzuki–Miyaura cross-coupling reaction with 2-thienylboronic acid in the presence of Na_2CO_3 as a base in anhydrous 1,4-dioxane under a nitrogen atmosphere *via* palladium catalysis to obtain the corresponding *N*-hydroxyethylated 3-thiophenyl carbazole **4** in 64% yield. The obtained thiophenyl carbazole primary alcohol **4** was subsequently phosphitylated by treatment with 2-cyanoethyl *N*,*N*-diisopropylchlorophosphoramidite in the presence of anhydrous ethyldiisopropylamine under an atmosphere of argon to afford the corresponding carbazole phosphoramidite **5** in 78% yield.

Due to its high sensitivity to humidity and light, the obtained thiophenyl carbazole phosphoramidite **5** was immediately used on an automated DNA synthesizer in order to synthesize the oligonucleotides **ON3** with the inserted carbazole monomer **Z** using the standard phosphoramidite approach (Table 1). The correct molecular weights of the synthesized ONs were verified by matrix-assisted laser desorption/ionization time-of-flight (MALDI-TOF) mass spectrometry, and the purity was verified as >90% according to ion exchange HPLC analysis.

Hybridization studies of duplexes: binding affinity and mismatch sensitivity

The influence of the non-nucleosidic thiophenyl carbazole monomer **Z** on the stability of various DNA/DNA and DNA/

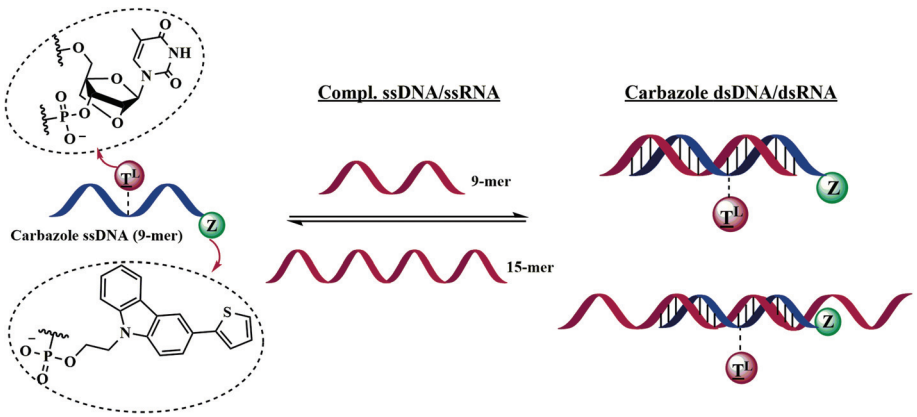

Fig. 1 Structures of the carbazole and LNA-T monomers employed, and the duplexes formed between the modified 9-mer ON and complementary DNA/RNA target strands.

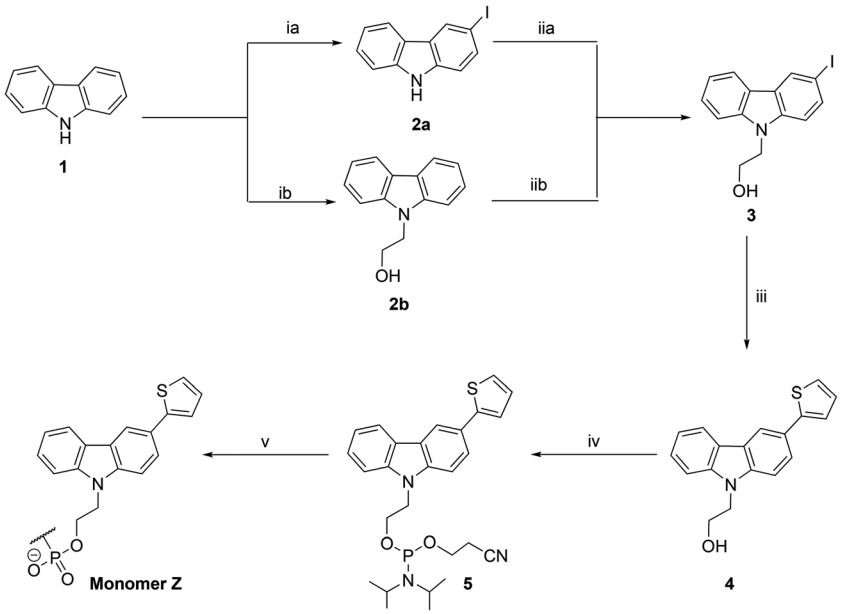

Scheme 1 Synthesis of carbazole intermediates and phosphoramidite monomer **5**. Reagents and conditions: (ia) IPy_2BF_4, $CuSO_4$, 65 °C, anhydrous CH_3CN, 10 min, 79%; (ib) KOH, anhydrous DMF, 30 min, RT, $Br(CH_2)_2OH$, 80 °C, 20 h, 83%; (iia) KOH, anhydrous DMF, 30 min, RT, $Br(CH_2)_2OH$, 80 °C, 20 h, 77%; (iib) IPy_2BF_4, $CuSO_4$, 65 °C, anhydrous CH_3CN, 10 min, 85%; (iii) 2-thienylboronic acid, anhydrous 1,4-dioxane, Na_2CO_3, $Pd(dppf)Cl_2$·DCM, 64%; (iv) $NC(CH_2)_2OP(NPr^i_2)Cl$, dry $EtN(Pr^i)_2$, dry DCM, RT, Ar, 2 h, 78%; (v) ON synthesis.

Table 1 T_m [a] (°C), ΔT_m [b] (°C) data for thermal denaturation temperatures of unmodified and modified DNA/DNA and DNA/RNA duplexes at 260 nm

Complementary sequence	Code	5′-GTG ATA TGC-3′ (**ON1**)	5′-GTG A**T^L**A TGC-3′ (**ON2**)	5′-**Z**GTG A**T^L**A TGC-3′ (**ON3**)
3′-CAC TAT ACG-5′	**D0**	32.2	38.0 (+5.8)	40.2 (+8.0)
3′-CAC UAU ACG-5′	**R0**	30.2	39.4 (+9.2)	39.0 (+8.8)
3′-**TTC** CAC TAT ACG **CTC**-5′	**D1**	36.2	42.0 (+5.8)	46.2 (+10.0)
3′-**UUC** CAC UAU ACG **CUC**-5′	**R1**	33.6	42.2 (+8.6)	42.0 (+8.4)

[a] Conditions: 2.5 μM of each strand in a medium salt buffer 5.8 mM NaH_2PO_4/Na_2HPO_4 buffer (pH 7.0), containing 100 mM NaCl and 0.10 mM EDTA. [b] The T_m values reflect the average of two measurements. Numbers in parentheses are differences in T_m (ΔT_m) = T_m (modified) − T_m (unmodified). Z = carbazole monomer, T^L = LNA-T monomer.

RNA duplexes was investigated by thermal denaturation experiments in medium salt buffer (2.5 μM concentration of each strand) at pH 7.0 using the UV melting method at 260 nm with thermal denaturation temperatures (T_m, °C) determined as the maximum of the first derivative plots. In this frame, the fully characterized nonamer 5′-GTGATATGC-3′ DNA sequence **ON1** was used in this study, in which the carbazole monomer **Z** was terminally incorporated into the 5′-end together with substitution of the central DNA-T nucleotide by an LNA-T monomer to give the sequence **ON3** (Table 1).

The binding affinity and specificity of the carbazole-modified oligonucleotide **ON3** were assessed towards both complementary 9-mer DNA and RNA strands (**D0** and **R0**, respectively) as well as towards 15-mer DNA and RNA strands (**D1** and **R1**, respectively) each having a three-nucleotide overhang at each end relative to the 9-mer central region designed to partake in duplex formation. These longer targets were included as models for longer more biologically relevant targets. More specifically we wished to evaluate the capability of the carbazole intercalator **Z** to undergo π–π stacking with surrounding nucleobases at the overhang regions in addition to exploring the intercalating effectiveness of monomer **Z** as a stacking lid stabilizing the 9-mer DNA/DNA and DNA/RNA duplexes. The T_m values obtained for the unmodified all-DNA 9-mer strand **ON1** and the central LNA-T modified 9-mer strand **ON2**, both hybridized with complementary 9-mer/15-mer single-stranded DNAs or RNAs, are considered as the control measurements referred for comparison. The T_m values of the carbazole-modified duplexes were recorded and compared with the T_m of the unmodified duplexes to determine the differences in melting temperatures (ΔT_m values, Table 1). The resulting denaturation duplex curves all displayed the expected monophasic sigmoidal transitions (Fig. S17, ESI†).

For possible perfectly matched 9-mer unmodified duplexes, all DNA reference **ON1** revealed a thermal denaturation temperature of 32.2 °C with the complementary DNA strand **D0** and 30.2 °C with the RNA counterpart **R0**, whereas the thermal melting temperature for the control LNA-T **ON2** was 38.0 °C

and 39.4 °C with the corresponding DNA and RNA complements, respectively. These values correspond to other measurements made earlier.[48] As can be seen from Table 1, the carbazole-modified DNA/DNA duplex **ON3**/**D0** forms a significantly more thermally stable duplex with ΔT_m 8.0 °C than the wild type DNA-T **ON1**/**D0**. In fact, this duplex is even more thermostable by +2.2 °C relative to the corresponding LNA-T control **ON2**/**D0** duplex indicating that the thiophenyl carbazole moiety is well accommodated at the 5′-end of the duplex. This stabilizing influence of the carbazole monomer **Z** is most likely attributable to favorable positioning of the aromatic polycyclic system for inter-strand stacking including the underlying nucleobases (known as the lid-effect). It should be noted that our aromatic carbazole lid has a duplex stabilizing effect relative to the pyrene twisted intercalating nucleic acid (TINA)[49] and for the phenanthroimidazole intercalator (Amany),[50] but similar to the intercalating nucleic acid (INA)[51] and the 2′-deoxyribose phenanthrene nucleotide at the 5′-end.[52]

The T_m value of the carbazole-modified DNA/RNA duplex **ON3**/**R0** was approximately 9.0 °C higher than the T_m value of the wild type duplex **ON1**/**R0**. However, the T_m decreased weakly by 0.4 °C compared to the corresponding duplex containing LNA-T only **ON2**/**R0**.

Hereafter, we investigated the hybridization of the carbazole-modified 9-mer sequence **ON3** with two target 15-mer ONs, *i.e.* DNA (**D1**) and RNA (**R1**) strands encompassing three unpaired nucleotides as overhangs at both ends of the parental 9-mer DNA and RNA complements. As is evident for the DNA/DNA duplexes (Table 1), again monomer **Z** and the LNA-T monomers induced similar increases as described above for all the 9-mer duplexes. However, relative to the LNA-T only modified duplex **ON2**/**D1**, the increased thermal stability even increased by 4.2 °C (Table 1), suggesting the favorable stacking interaction from the large aromatic surface of the carbazole intercalator with nucleobases anchored as overhangs, and not only acting as lids, into the 15-mer DNA complement. Again, similar trends were detected with RNA strands as targets where the lack of any stabilizing effect originating from the carbazole moiety is hypothesized to be due to inefficient intercalation of monomer **Z** into the DNA/RNA duplex **ON3**/**R1**, as has been earlier observed with other intercalating units.[51,53]

Based on the above data, we conclude that the carbazole-based monomer **Z** is well fitted as 5′-end modification to engage in stabilizing interactions within the B-type helix geometry of a DNA/DNA duplex, whereas neither stabilizing nor destabilizing interactions are observed for a corresponding DNA/RNA duplex likely adopting an A/B-type helical structure.

In order to assert the formation of all 9-mer/15-mer carbazole hybrids and unmodified duplexes, circular dichroism (CD) spectra were recorded. For all carbazole-modified DNA/DNA duplexes (**ON3**/DNA) as well as LNA-T modified counterparts (**ON2**/DNA), CD spectra displayed intense positive and negative amplitudes at ~280 nm and ~250 nm, respectively, with no major variations relative to those of the unmodified duplexes **ON1**/DNA. Such data are consistent with the characteristic features of a DNA B-conformation (Fig. S18, ESI†). In parallel, the CD spectra of carbazole-modified DNA/RNA variants (**ON3**/RNA) revealed the characteristic profile of an intermediate A/B-type helical environment with ellipticities from both geometries. Thus, positive bands of strong intensity at ~265 nm (A-type) with a shoulder at ~280 nm (B-type) were recorded along with negative bands of rather low intensities at ~240 nm and ~210 nm (A-type). The intensity of the bands is not significantly changed relative to those of the unmodified DNA/RNA duplexes **ON1**/RNA suggesting that the carbazole monomer does not induce any changes in the overall A/B-type duplex structure (Fig. S18, ESI†).

As a next step, we investigated the binding specificity of the carbazole-modified oligonucleotide **ON3** using 15-mer **D1** and **R1** as targets with overhangs and two types of mismatched nucleotides. The capability for mismatch discrimination was first examined by comparing the melting temperatures of DNA/DNA duplexes **ON1–ON3**/**D2–D7** and DNA/RNA duplexes **ON1–ON3**/**R2–R7**, focusing on a mismatch (either in the juxtaposition or in a directly opposite position to the carbazole-functionalized monomer **Z**) with the melting temperatures of the corresponding fully matched duplexes **ON1–ON3**/**D1** and **ON1–ON3**/**R1** (ΔT_m values).

The first type of mismatch was specifically introduced at position 13 of **D1** and **R1** complementary strands directly opposite to the monomer **Z** in **ON3**, *i.e.* in the first overhang position relative to the nine-mer fully matched duplex segment. As outlined in Table 2, when the cytosine nucleobase was replaced by the purines adenine or guanine, a small increase in T_m ranging from 0.8 °C to 2.4 °C (for **ON1–ON3**/**D2**, **D3** duplexes) and from 2.2 °C to 4.4 °C (for **ON1–ON3**/**R2**, **R3** duplexes) was detected relative to their perfectly matched duplexes. However, these increases were less pronounced than that obtained with the non-carbazole containing duplexes used as controls (**ON1** and **ON2**). Negligible mismatch discriminations were observed when the cytosine nucleobase was replaced by the pyrimidine bases thymine (**ON1–ON3**/**D4**) or uracil (**ON1–ON3**/**R4**). These data show that monomer **Z** positioned as in these systems is unable to induce stabilizing stacking effects (Fig. S19 and S20, ESI†).

Next, mismatches were also present in position 12 of the target strands substituting the relevant cytosine base (**D5–D7** for DNA and **R5–R7** for RNA). All possible mismatches in the **D1**/**R1** targets at position 12 resulted in significant mismatch recognition (ΔT_m = 7.6–11.4 °C for DNA/DNA duplexes and ΔT_m = 8.2–20.4 °C for DNA/RNA duplexes) as depicted in Table 2. In the case of the mismatched DNA/DNA duplexes, the highest ΔT_m value of discrimination displayed by the **ON1**/**D5** duplex was 11.4 °C for replacement of C by G, and 10.2–10.0 °C displayed by carbazole-functionalized duplexes **ON3**/**D5**, **D6** upon substituting C with G or A (Fig. S21, ESI†), while for mismatched DNA/RNA duplexes, the highest value of discrimination was observed for the **ON1**/**R5** duplex (20.4 °C upon replacement of C by G; Fig. S22, ESI†). Surprisingly, the mismatched DNA/RNA duplex **ON1**/**R5** showed an S-shaped melting curve using a medium salt buffer. To unveil this unclear transition, thermal denaturation experiments were

Table 2 T_m [a] (°C), ΔT_m [b] (°C) data for thermal denaturation temperatures at 260 nm of the matched and mismatched duplexes involving complementary DNA and RNA strands with mismatches directly opposite to modification (positions 12 and 13)

Code DNA/RNA[c]	Complementary sequence 3′-TT**B** CAC TAT ACG CTC-5′	B (DNA) C **D1**	G **D2**	A **D3**	T **D4**	B (RNA) C **R1**	G **R2**	A **R3**	U **R4**
ON1	5′-GTG ATA TGC-3′	36.2	+2.4	+1.8	+0.2	33.6	+3.4	+4.4	+0.6
ON2	5′-GTG AT^{L}A TGC-3′	42.0	+1.8	+2.2	±0.0	42.2	+3.6	+4.2	+0.8
ON3	5′-**Z**GTG AT^{L}A TGC-3′	46.2	+0.8	+0.8	-0.4	42.0	+2.2	+2.2	±0.0

Code DNA/RNA[c]	Complementary sequence 3′-TTC **B**AC TAT ACG CTC-5′	B (DNA) C **D1**	G **D5**	A **D6**	T **D7**	B (RNA) C **R1**	G **R5**	A **R6**	U **R7**
ON1	5′-GTG ATA TGC-3′	36.2	−11.4	−9.8	−8.0	33.6	−20.4	−10.0	−9.6
ON2	5′-GTG AT^{L}A TGC-3′	42.0	−9.4	−9.0	−7.6	42.2	−11.8	−8.4	−8.2
ON3	5′-**Z**GTG AT^{L}A TGC-3′	46.2	−10.0	−10.2	−8.2	42.0	−10.6	−9.2	−8.8

[a] Conditions: 2.5 μM of each strand in a medium salt buffer 5.8 mM NaH_2PO_4/Na_2HPO_4 buffer (pH 7.0), containing 100 mM NaCl and 0.10 mM EDTA. [b] The T_m values reflect the average of two measurements. ΔT_m values for mismatches were calculated as the difference in T_m values between the mismatched and fully matched duplexes. [c] In RNA targets, the uracil bases are present instead of the thymine bases. Z = carbazole monomer, T^{L} = LNA-T monomer and B are bases mismatched to duplexes.

performed for **ON1**/(**R1**, **R5**, **R6** and **R7**) in a high salt buffer concentration containing 1 M (instead of 100 mM) NaCl. The resulting melting curves displayed clear sigmoidal transitions with similar (ΔT_m = 9.0–9.4 °C, **ON1**/**R6**, **R7**) or slightly lower (ΔT_m = 16.8 °C, **ON1**/**R5**) mismatch discrimination when compared to the values measured at a medium salt concentration (Table 3 and Fig. 2, Fig. S23 ESI†).

Generally, the mismatched carbazole duplexes demonstrated similar (DNA/DNA duplex; **ON3**/**D5**–**D7**) or substantially lower (DNA/RNA duplex; **ON3**/**R5**–**R7**) mismatch discrimination relative to the corresponding mismatched reference duplexes containing **ON1** and **ON2**.

To study the structural features of all mismatched reference as well as carbazole modified duplexes in detail, CD spectroscopy was employed. All the mismatched dsDNA duplexes are of the B-form with positive maxima around 280 nm and negative minima around 250 nm. As expected for all mismatched DNA/RNA duplexes, CD spectra imply no major structural variations in the overall A/B-form duplex with positive peaks around 265 nm and two negative ones around 240 nm and 210 nm with similar amplitudes (except for **D5** and **D7**) (Fig. S24–S27 ESI†).

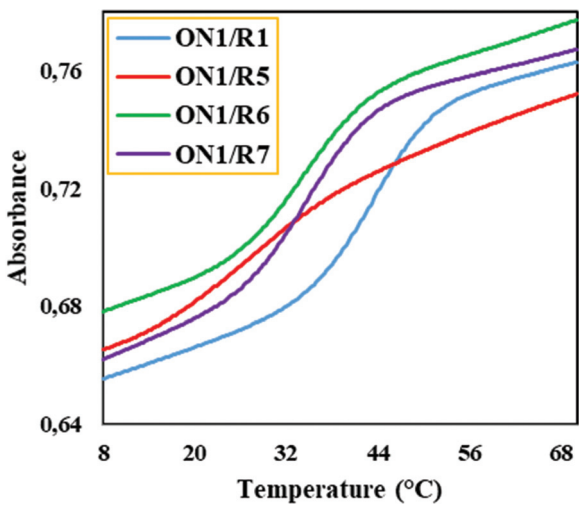

Fig. 2 UV melting curves of matched and mismatched DNA/RNA duplexes with mismatches at position 12. Conditions are described in Table 3. **R1** is a fully matched DNA/RNA duplex, while **R5**, **R6** and **R7** are mismatched DNA/RNA duplexes.

Table 3 T_m [a] (°C), ΔT_m [b] (°C) data for thermal denaturation temperatures at 260 nm of matched (**R1**) and mismatched DNA/RNA duplexes (R5–R7) at high salt concentration

Complementary sequence	Code	5′-GTG ATA TGC-3′(ON1)
3′-**UUC** CAC UAU ACG **CUC**-5′	**R1**	43.8
3′-**UUC** G̲AC UAU ACG **CUC**-5′	**R5**	27.0 (−16.8)
3′-**UUC** A̲AC UAU ACG **CUC**-5′	**R6**	34.4 (−9.4)
3′-**UUC** U̲AC UAU ACG **CUC**-5′	**R7**	34.8 (−9.0)

[a] Conditions: 2.5 μM of each strand in a high salt buffer 5.1 mM NaH_2PO_4/Na_2HPO_4 buffer (pH 7.0), containing 1 M NaCl and 0.10 mM EDTA. [b] The T_m values reflect the average of two measurements. Numbers in parentheses are differences in T_m (ΔT_m) = T_m (mismatched) − T_m (matched). The underlined bases are mismatched to duplexes.

Fluorescence studies for carbazole containing ONs

The steady-state fluorescence emission spectra of the carbazole-modified single-strand **ON3**, and the full spectrum of the matched and mismatched carbazole DNA/DNA and DNA/RNA duplexes were recorded using excitation of the carbazole moiety at 310 nm. In all cases, the fluorescence spectra were scanned from 350 to 600 nm in the same buffer solutions as used for UV thermal melting studies. ONs containing carbazole monomer **Z** displayed characteristic emission maxima

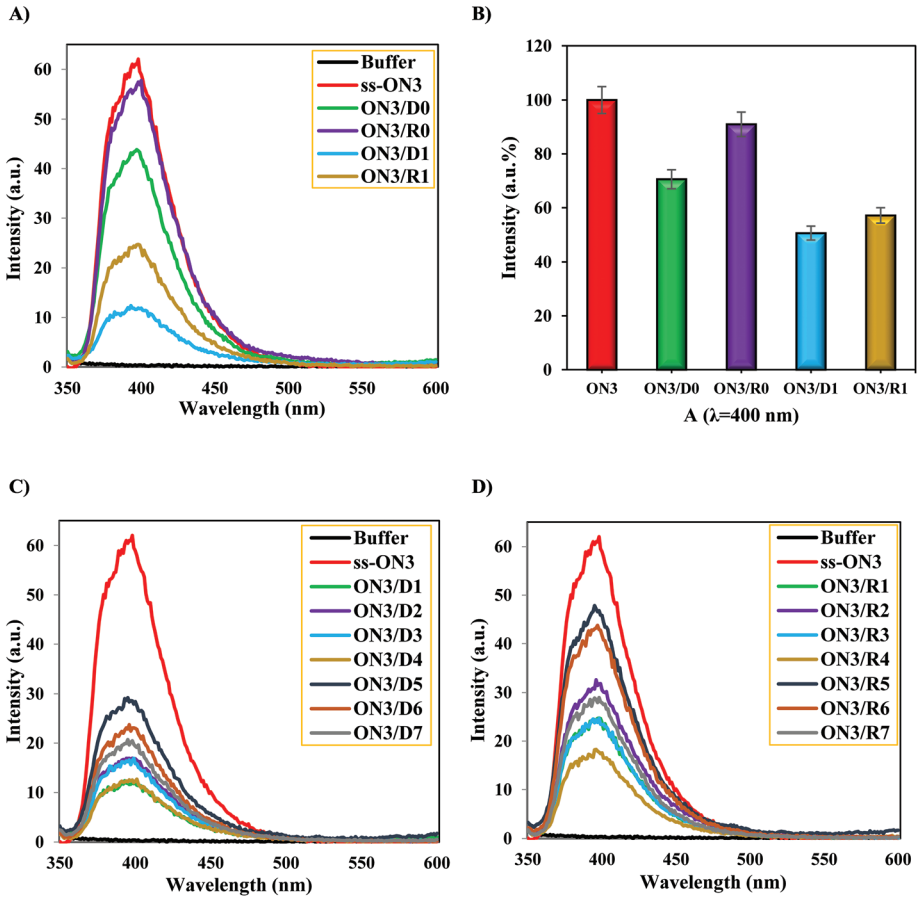

Fig. 3 (A) Steady-state fluorescence emission spectra of the carbazole single-strand (**ss-ON3**), and its matched duplexes with complementary DNA and RNA. (B) Fluorescence intensities for the matched carbazole modified duplexes and their remaining percentages at 400 nm relative to **ON3**. (C) Steady-state fluorescence emission spectra of the carbazole single-strand (**ss-ON3**), the fully matched DNA/DNA carbazole duplex **ON3/D1**, and mismatched DNA/DNA carbazole duplexes (**ON3/D2–D7**). (D) Steady-state fluorescence emission spectra of the carbazole single-strand (**ss-ON3**), fully matched DNA/RNA carbazole duplex **ON3/R1**, and mismatched DNA/RNA carbazole duplexes (**ON3/R2–R7**). All fluorescence measurements were obtained using 2.5 μM concentrations of the two strands in a medium salt buffer (5.8 mM NaH_2PO_4/Na_2HPO_4 buffer (pH 7.0), containing 100 mM NaCl and 0.10 mM EDTA) at 20 °C; λ_{ex} = 310 nm.

around 400 nm (representative fluorescence spectra are shown in Fig. 3). For all possible matched carbazole duplexes, the fluorescence emission intensity was typically quenched upon hybridization with DNA/RNA targets with more pronounced decreases typically being observed upon DNA binding (Fig. 3A and B). Interestingly, the 9-mer matched carbazole duplexes without overhangs (**ON3/D0** and **ON3/R0**) are noticeably more fluorescent than the matched carbazole duplexes (**ON3/D1** and **ON3/R1**) containing 15-mer complementary sequences. This indicates that the carbazole moiety **Z**, when positioned at the 5′-end of the 9-mer ON, interacts strongly upon hybridization, most likely *via* intercalation leading to quenched fluorescence.

Thereafter, the fluorescence properties of carbazole duplexes formed by **ON3** and mismatched DNA/RNA targets were investigated (Fig. 3C and D). Generally, probe **ON3** was seen to be highly sensitive to the presence of mismatched nucleotides in DNA than RNA targets for both types of mismatches (at positions 12 or 13), showing 2.2–5.0 fold decreases in fluorescence intensities for mismatched DNA/DNA duplexes and between 1.3- to 3.5 fold for DNA/RNA mismatches relative to the fluorescence obtained for the single-stranded probe **ON3**. Specifically, when a mismatch was due to G (**D2** and **R2**) or A (**D3**) opposite to the insertion of monomer **Z**, significant hybridization-induced decreases in carbazole monomer fluorescence intensities were observed upon mixing with **ON3**. Only the carbazole mismatched **ON3/R3** displayed the same fluorescence intensities in reference with the fully matched **ON3/R1**. It is noteworthy that the decreases in fluorescence emission intensities of mismatches in juxtaposition to the carbazole monomer upon mixing with **ON3** are generally less distinct than the decreases observed for mismatches directly opposite to monomer **Z**. The fluorescence properties for carbazole single-strand **ON3** suggest this to be an interesting new probe scaffold for selective detection of DNA and RNA target strands.

Molecular modeling of probe–target duplexes

To gain more insight into the efficacy of thiophenyl carbazole monomer **Z** to stabilize the duplex *via* intercalation, and

implicitly to further interpret the variations in T_m values, modeling calculations were carried out on the fully matched duplexes formed between the 9-mer **ON3** sequence and complementary 15-mer **D1**/**R1** strands. This would also give some information about the capability of the thiophenyl carbazole moiety to undergo π–π stacking interactions with surrounded-ing nucleobases. A modified AMBER* force field in Macro Model 9.2 molecular modeling was subjected to dynamics simulation and minimization in order to generate the representative low-energy structures of the modified duplexes. For the fully matched DNA duplex **ON3**/**D1**, a standard B-type DNA/DNA duplex conformation was built with subsequent incorporations of **Z** and LNA-T monomers into **ON3**, and trimer overhang nucleotides into **D1** (for details, see the Experimental section). While for the DNA/RNA **ON3**/**R1** hybrid, the starting NMR duplex solution structure was initially downloaded from the Protein Data Bank, code 1HHW[54] accession number and corrected, followed by terminal insertions of **Z** monomer into **ON3** and overhangs into **R1** (for details, see Experimental procedures). In agreement with the modeling simulation presented below for **Z**-modified DNA duplex structure **ON3**/**D1**, the carbazole moiety in monomer **Z** (cyan) is positioned nicely on the top of the underlying guanosine of the Watson–Crick 9-mer duplex *via* the π–π stacking interaction, whereas the thiophene ring in **Z** (magenta) interacts with the two adjacent up and down cytosines in a manner that facilitate more favourable π–π interactions, and thus remains stably intercalated in the duplex core as depicted in Fig. 4. In addition, the capability of twisting the aromatic moieties of the **Z** intercalator around the single bond allows them to adjust their positions to the local secondary structure of the duplex. This clearly means that thiophenyl carbazole intercalator **Z**, which behaves as a further base pair, is well-accommodated into the DNA duplex. Based on these data, we speculate that the appropriate intercalation modes together with the stacking properties contribute, together with the LNA nucleotide, to the 10.0 °C increase in T_m for **ON3**/**D1** when compared to the native duplex. Along the same line the 4.2 °C increase in T_m for **ON3**/**D1** when compared to the LNA-containing duplex **ON2**/**D1** underlines the affinity enhancing effect of monomers **Z**.

Conversely, in the case of the **Z**-modified DNA/RNA **ON3**/**R1** hybrid, the structural conformation of the thiophenyl carbazole building block **Z** is considerably changed. Molecular modeling depicts that the carbazole moiety (cyan) in **Z** is positioned substantially outward the duplex core and consequently no clear π–π stacking interactions with the underlying guanine nucleobase are rendered possible. Whereas the thiophene ring (magenta) is twisted to a large extent, in comparison with the carbazole moiety, stacking interactions with the surrounding cytosines appear weak at best which weaken the intercalating

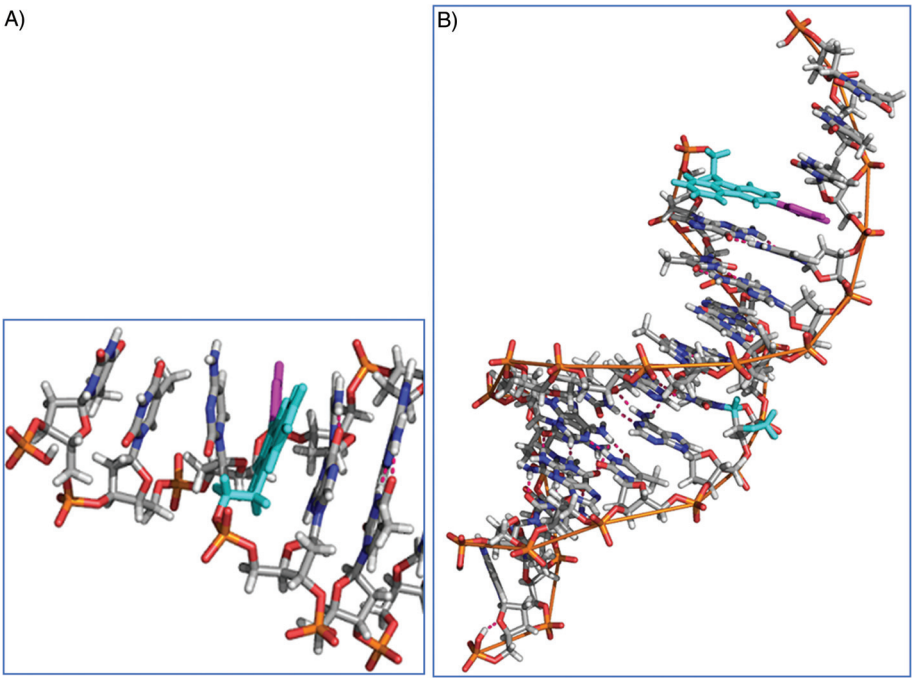

Fig. 4 Representative low-energy conformations of the fully matched carbazole-modified DNA/DNA duplex **ON3**/**D1** adopted between the 9-mer sequence: 5′-Z**G**T**G**A**T**^{L}A**T**G**C**-3′ (**ON3**) and its complementary 15-mer strand: 3′-**TTC**CAC TATACG**CTC**-5′ (**D1**) produced by an Amber*-minimized model. (A) Side view displaying hybridization and stacking mode interactions between thiophenyl carbazole monomer **Z** and the surrounding nucleobases of dsDNA. (B) Overall view displaying stacking interactions and overlapping for the possible conformation of **ON3**/**D1**. The carbazole moiety in monomer **Z** is shown in cyan, the thiophene ring in **Z** is shown in magenta, and LNA-T centrally inserted in **ON3** is marked in cyan. Hydrogen bonds between the canonical nucleobases are displayed in red. Guanosines, cytosines, adenines, and thymidines are displayed in their standard colors.

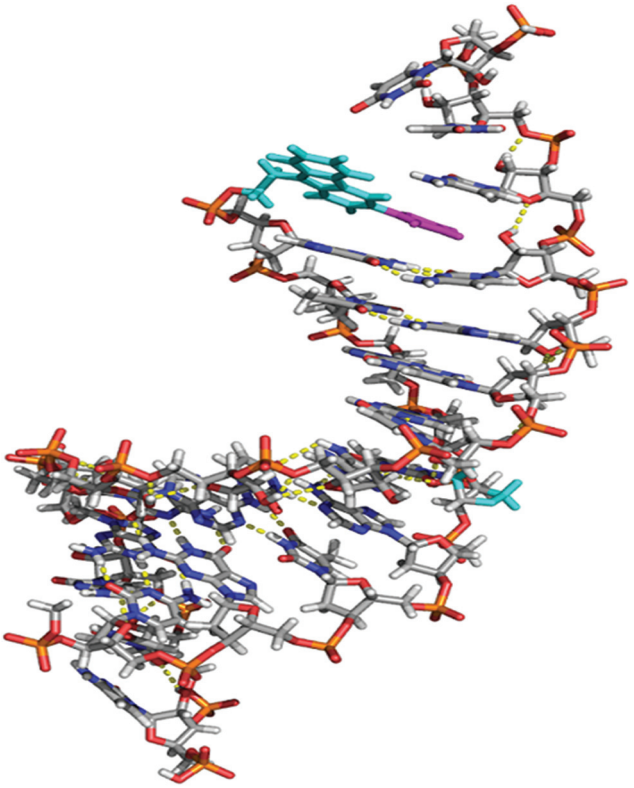

Fig. 5 Representative low-energy conformations of the fully matched carbazole-modified DNA/RNA hybrid duplex **ON3**/**R1** formed between the 9-mer sequence: 5′-**Z**GTGAT^{L}ATGC-3′ (**ON3**) and its complementary 15-mer strand: 3′-**UUC**CAC UAUACG**CUC**-5′ (**R1**) produced by an Amber*-minimized model. The carbazole moiety in monomer **Z** is shown in cyan, the thiophene ring in **Z** is shown in magenta, and LNA-T centrally inserted in **ON3** is marked in cyan. Hydrogen bonds between the canonical nucleobases are displayed in yellow. Guanosines, cytosines, adenines, thymidines and uridines are displayed in their standard colors.

efficiency of **Z** towards the DNA/RNA hybrid (Fig. 5). Another noteworthy observation is that the large extent of twisting of the thiophene ring as well as its inefficient intercalation into the **ON3**/**R1** duplex is ascribed to the presence of the negatively charged hydroxyl group of the opposite cytidine ribosugar (C_{12}) located in very close proximity to the negatively charged sulfur of the thiophene ring in **Z**. Such a type of electrostatic repulsion precludes the interior accommodation of the thiophene moiety into the helical DNA/RNA structure, and hence, reflects the inability of **Z** monomer to intercalate between the up and down cytosines. Another reason perturbing the intercalating properties of **Z** is the unfavorable steric clashes and/or strain within the DNA/RNA duplex construct which impair the interactions with the neighboring nucleobases. This entails the equivalency of thermostability observed for the carbazole-modified duplex **ON3**/**R1** and the corresponding LNA-T control duplex **ON2**/**R1** where LNA-T (cyan) is oriented towards the major groove of the double helix, adding to the stability of the DNA/RNA duplex.

Conclusions

Synthesis of a novel thiophenyl carbazole intercalating building block suitable for solid-supported DNA synthesis was developed *via* Suzuki–Miyaura cross-coupling. This building block was used on an automated nucleic acid synthesizer for 5′-end incorporation of monomer **Z** into a 9-mer sequence. This 9-mer displayed high-affinity hybridization towards complementary 9-mer/15-mer DNA and comparable affinity toward the corresponding RNA complements. With matched and singly mismatched DNA and RNA 15-mer targets, the carbazole containing 9-mer probe was able to signal full target complementarity using fluorescence spectroscopy, although the quenching was more profound than in the cases of DNA/RNA hybrids. Evident increases of fluorescence intensities were revealed upon hybridization of the carbazole single-strand probe with all 9-mer complements rather than all 15-mer complements encompassing overhangs. Based on modeling studies, the increased thermal stabilities and the fluorescence quenching observed for **Z**-modified DNA/DNA duplexes are suggested to be a result of efficient π–π stacking interactions. The interesting fluorescence profiles reported herein, taken together with high-affinity binding and mismatch sensitivity to complementary targets, make ONs containing carbazole monomer **Z** as dangling 5′-end modification a new design for exploitation within nucleic acid diagnosis and in nucleic acid targeting.

Experimental section

All reactions were carried out under a N_2 or Ar atmosphere using anhydrous solvents and glassware that had been dried at 120 °C. Column chromatography was carried out under pressure using Merck Millipore silica gel 60 (0.040–0.063 mm). Analytical silica gel thin layer chromatography (TLC) was performed using Merck Kieselgel 60 F_{254} (0.22 mm thickness, precoated aluminum plates). The silica was pretreated with a solvent containing 1% Et_3N, and dried over activated molecular sieves (3 Å, 2–3 mm), for compounds sensitive to acids. All reagents used were purchased from Sigma-Aldrich, Fluka and used without purification. Dichloromethane (DCM), *N*,*N*-diisopropylethylamine (DIPEA), *N*,*N*-dimethylformamide (DMF), and ethyl acetate (AcOEt) were dried over activated molecular sieves (4 Å, 2–3 mm) and measured on a Karl Fischer titrator (<12 ppm). Petroleum ether: bp. 60–80 °C, triethylamine (Et_3N) and acetonitrile (CH_3CN) were dried over activated molecular sieves (3 Å, 2–3 mm). Acetone and ethanol were used as received. Barluenga's reagent (IPy_2BF_4) was synthesized in a safe and scalable procedure from iodine, pyridine and silver salt according to the procedure reported by Davis *et al.*[55]

NMR spectra were recorded for compounds **5** at room temperature on a Bruker AVANCE III 400 spectrometer at 400 MHz for ^{1}H, 101 MHz for ^{13}C, and at 162 MHz for ^{31}P with TMS as an internal standard for ^{1}H NMR. For compounds **2**–**4**, NMR spectra were recorded at 298 K on an Agilent NMR Magnet-

400 MHz (399.89 MHz for ^{1}H and at 100.56 MHz for ^{13}C). Chemical shifts are reported in parts per million (δ), relative to the residual non-deuterated solvents peaks ($CDCl_3$: 7.26 ppm for ^{1}H and 77.16 ppm for ^{13}C; DMSO-d_6: 2.50 ppm for ^{1}H and 39.5 ppm for ^{13}C; 85% aq. H_3PO_4 as an external standard with 0.00 ppm for ^{31}P NMR). Multiplicities are abbreviated as follows: s = singlet, d = doublet, t = triplet, m = multiplet. For the final phosphoramidite **5**, the spectral assignment for ^{1}H NMR and ^{13}C NMR has been confirmed by H–H correlation (COSY), H–C correlation (HSQC) and long-range H–C correlation (HMBC). High-resolution electrospray ionization mass spectroscopy (ESI-MS) experiments were performed for compounds **2a**, **2b** and **3** using a Waters Xevo G2 QTOF instrument equipped with an injection system (cone voltage 50 V; source 120 °C). For compounds **3** and **4**, electrospray ionization high-resolution mass spectra (ESI-HRMS) were obtained on a Bruker APEX III FT-ICR mass spectrometer using chloroform or acetonitrile as the solvent. For accurate ion mass determination, the ($M + H^+$) or ($M + Na^+$) ions were peaks matched by calibration with NaI. Melting points were determined with a Boetius apparatus and are not corrected. Elemental analysis was conducted with the PerkinElmer 2400 Series II CHNS/O Elemental Analyzer. The progress of the reactions was monitored by thin-layer chromatography (TLC) using silica gel coated aluminum plates with a fluorescence indicator (Merck, SiO_2 60, F254) and visualized with UV light (254 and 365 nm) or dipping into a solution of vanillin (400 mg of vanillin in 200 mL of EtOH, 4 mL of H_2SO_4).

Commercially available DNA phosphoramidite monomers, solid supports, additional reagents and the wild types DNA, as well as RNA oligonucleotides, were purchased from Sigma-Aldrich, Glen Research or GE Healthcare. Acetonitrile and 5-[3,5-bis(trifluoromethyl)phenyl]-1*H*-tetrazole, required for the hand coupling step, were dried over activated molecular sieves (3 Å, 2–3 mm) and their dryness was measured on a Karl Fischer titrator (<10 ppm). The synthesized oligonucleotides were purified by IE-HPLC with HPLC grade acetonitrile or methanol as the solvent. The composition of the synthesized oligonucleotide was verified by MALDI-TOF analysis on a Bruker Daltonics Microflex *LT* (MALDI-LIFT system) MS instrument in ES^+ mode with the HPA matrix (10 mg 3-hydroxypicolinic acid in 50 mM ammoniumcitrate/70% acetonitrile).

3-Iodo-9*H*-carbazole (2a)[46]

Carbazole (5.01 g, 30.0 mmol) was added to a solution of IPy_2BF_4 (12.27 g, 33.0 mmol) and $CuSO_4$ (270 mg, 1.65 mmol) under a N_2 atmosphere (Schlenk line) in anhydrous acetonitrile (50 mL) and the solution turned deep blue. The reaction was stirred at 65 °C for 10 min and then diluted with 90 mL of a sat. sodium thiosulfate solution. The precipitate formed was filtered off and rinsed with distilled water. The solid was dried in a vacuum desiccator over P_2O_5. The crude product contained a trace amount of the 3,6-diiodo-9*H*-carbazole byproduct. The product was recrystallized from hot water. The 3-iodo-9*H*-carbazole was obtained as a white-cream solid (6.95 g, 23.7 mmol, 79% yield); mp 193 °C (lit.[56] mp 192–194 °C). ^{1}H NMR (DMSO-d_6) δ (ppm): 7.17 (ddd, J = 8.0, 7.1, 1.0 Hz, 1H), 7.34 (d, J = 8.5 Hz, 1H), 7.42 (d, J = 7.1 Hz, 1H), 7.49 (dd, J = 8.0, 1.0 Hz, 1H), 7.63 (dd, J = 8.5, 1.8 Hz, 1H), 8.15 (dd, J = 8.0, 1.0 Hz, 1H), 8.50 (d, J = 1.8 Hz, 1H), 11.38 (s, 1H, NH). ^{13}C NMR (DMSO-d_6) δ (ppm): 81.3 ($C_{aro.}$-I), 111.0, 113.4, 118.9, 120.6, 121.1, 125.1, 126.2, 128.6, 133.3, 138.7, 139.7 ($C_{aro.}$). HRMS (ESI) m/z $[M + H]^+$ calcd for $C_{12}H_9IN$: 293.9779, found 293.9780. Anal. Calcd for $C_{12}H_8IN$: C, 49.17; H, 2.75; N, 4.78. Found: C, 49.04; H, 2.87; N, 4.63.

2-(9*H*-Carbazol-9-yl)ethan-1-ol (2b)[47]

The synthetic method for compound **2b** is optimized and fully characterized in this report. Powdered potassium hydroxide (14.0 g) was stirred with DMF (80 mL) at room temperature for 10 min. The mixture was then stirred with carbazole (6.6 g, 0.040 mol) at room temperature for 45 min. 2-Bromoethanol (3.5 mL, 0.05 mol) was added slowly, and the resultant mixture was allowed to stir at room temperature for 10 h. The mixture was poured into water (1.2 L), and the white solid was filtered, washed with water, and air dried. The white solid was dissolved in 70% ethanol, and the insoluble residue was filtered out. Water was added to the filtrate until the precipitation was completed. The precipitate was filtered and dried under vacuum. Yield: 83% (6.95 g) as a white solid; mp 80 °C. ^{1}H NMR ($CDCl_3$) δ (ppm): 1.63 (bs, 1H, NCH_2CH_2OH), 3.94 (d, J = 5.3 Hz, 2H, NCH_2CH_2OH), 4.34–4.47 (m, 2H, NCH_2CH_2OH), 7.19–7.26 (m, 2H), 7.38–7.49 (m, 4H), 8.06 (d, J = 7.8 Hz, 2H). ^{13}C NMR ($CDCl_3$) δ (ppm): 45.6 (NCH_2CH_2OH), 61.6 (NCH_2CH_2OH), 108.9, 119.3, 120.5, 123.1, 125.9, 140.8 ($C_{aro.}$). MS (ESI) m/z $[M + H]^+$ calcd for $C_{14}H_{13}NO$: 212.11, found 212.11. Anal. Calcd for $C_{14}H_{13}NO$: C, 79.59; H, 6.20; N, 6.63. Found: C, 79.69; H, 6.07; N, 6.44.

2-(3-Iodo-9*H*-carbazol-9-yl)ethan-1-ol (3)

Method A. To a solution of 3-iodocarbazole (**2a**, 1.47 g, 5.02 mmol) in anhydrous DMF (25 mL), potassium hydroxide (2.25 g, 40.16 mmol) was added while stirring. The reaction mixture was stirred for 30 min at room temperature and 2-bromoethanol (540 μL, 7.55 mmol) was slowly added (approx. 45 min). The temperature was increased to 80 °C and stirring was continued for 20 h. The reaction mixture was cooled down to room temperature and poured into water (300 mL). The precipitate was filtered off and recrystallized from ethanol. Yield: 77% (1.31 g) as a pale beige solid.

Method B. 2-(9*H*-Carbazol-9-yl)ethan-1-ol (**2b**, 3.17 g, 15.0 mmol) was added to a solution of IPy_2BF_4 (6.14 g, 16.5 mmol) and $CuSO_4$ (135 mg, 0.83 mmol) under a N_2 atmosphere (Schlenk line) in anhydrous acetonitrile (25 mL), and the solution turned deep blue. The reaction was stirred at 65 °C for 10 min and then diluted with 42 mL of a sat. sodium thiosulfate solution. The precipitate formed was filtered off and rinsed with distilled water. The solid was dried in a vacuum desiccator over P_2O_5. Yield: 85% (4.31 g) as a white-cream solid; mp 105–108 °C. ^{1}H NMR ($CDCl_3$) δ (ppm): 1.57 (bs, 1H, NCH_2CH_2OH), 3.99 (m, 2H, NCH_2CH_2OH), 4.39 (t, J = 5.3 Hz, 2H, NCH_2CH_2OH), 7.22 (d, J = 8.2 Hz, 1H), 7.24 (d, J =

6.7 Hz, 1H), 7.42 (d, J = 8.2 Hz, 1H), 7.46 (d, J = 7.2 Hz, 1H), 7.68 (d, J = 7.2 Hz, 1H), 8.00 (d, J = 7.8 Hz, 1H), 8.37 (s, 1H). ^{13}C NMR ($CDCl_3$) δ (ppm): 45.6 (N*C*H_2CH$_2$OH), 61.5 (NCH$_2$*C*H$_2$OH), 81.8 ($C_{aro.}$-I), 109.1, 111.1, 119.8, 120.7, 121.8, 125.6, 126.7, 129.0, 134.8, 140.0, 140.7 ($C_{aro.}$). HRMS (ESI) m/z $[M + H]^+$ calcd for $C_{14}H_{13}INO$: 338.0041, found 338.0043. Anal. Calcd for $C_{14}H_{12}INO$: C, 49.87; H, 3.59; N, 4.15. Found: C, 50.03; H, 3.58; N, 4.11.

2-(3-(Thiophen-2-yl)-9*H*-carbazol-9-yl)ethan-1-ol (4)

To a suspension of 2-(3-iodo-9*H*-carbazol-9-yl)ethan-1-ol (**3**, 1.02 g, 3.0 mmol) in anhydrous 1,4-dioxane (10 mL), 2-thienylboronic acid (0.576 g, 4.5 mmol) was added while stirring; then 2 M Na_2CO_3 (3 mL) and the Pd(dppf)Cl_2·DCM [1,1′-bis (diphenylphosphino)ferrocene]dichloropalladium(II) complex with dichloromethane (0.196 g, 0.24 mmol) were added. The reaction mixture was placed in Schlenk line and after degassing it was refluxed under nitrogen for 18 h. After that time the reaction mixture was concentrated under reduced pressure and purified using a silica gel packed column using petroleum ether : ethyl acetate (3 : 1 to 7 : 3 v/v). Yield: 64% (0.806 g) as a white powder; mp 120–122 °C. ^{1}H NMR ($CDCl_3$) δ (ppm): 1.59 (bs, 1H, NCH$_2$CH$_2$O*H*), 3.99 (t, 2H, NCH$_2$C*H*$_2$OH), 4.41 (t, J = 5.6 Hz, 2H, N*C*H_2CH$_2$OH), 7.09 (dd, J = 4.8 Hz, J = 3.6 Hz, 1H, $H_{thio.}$), 7.22–7.26 (m, 2H), 7.32 (dd, J = 3.6, 1.1 Hz, 1H), 7.39–7.47 (m, 3H), 7.69 (dd, J = 8.4 Hz, J = 1.6 Hz, 1H, $H_{thio.}$), 8.10 (d, J = 7.6 Hz, 1H), 8.29 (d, J = 1.6 Hz, 1H). ^{13}C NMR ($CDCl_3$) δ (ppm): 45.7 (N*C*H_2CH$_2$OH), 61.6 (NCH$_2$*C*H$_2$OH), 109.1, 109.3, 118.0, 119.6, 120.7, 122.3, 123.1, 123.5, 123.9, 124.6, 126.3, 126.3, 128.1, 140.4, 141.3, 145.7 ($C_{aro.}$). HRMS (ESI) m/z $[M + H]^+$ calcd for $C_{18}H_{16}NOS$: 294.0952, found 294.0953. Anal. Calcd for $C_{18}H_{15}NOS$: C, 73.69; H, 5.15; N, 4.77. Found: C, 73.50; H, 4.93; N, 4.49.

2-Cyanoethyl (2-(3-(thiophen-2-yl)-9*H*-carbazol-9-yl)ethyl) diisopropylphosphoramidite (5)

The alcohol **4** (0.293 g, 1.0 mmol) was coevaporated with anhydrous acetonitrile (3 × 20 mL) and dissolved together with anhydrous *N*,*N*-diisopropylethylamine (0.33 g, 2.55 mmol) under an argon atmosphere in anhydrous dichloromethane (10 mL). 2-Cyanoethyl-*N*,*N*-diisopropylchlorophosphoramidite (0.284 g, 1.2 mmol) dissolved in anhydrous dichloromethane (5 mL) was added dropwise, and the reaction mixture was stirred at room temperature for 2 h. The resulting mixture was transferred with a dry syringe and directly applied onto the top of a silica gel column for purification under super dry conditions (AcOEt : TEA 99 : 1 v/v). The phosphoramidite is sensitive to moisture and light and it was immediately used for DNA synthesis. Yield: 78% (0.385 g) as a yellow semi-solid. R_f = 0.32 (99 : 1 AcOEt/TEA v/v). ^{1}H NMR (DMSO-d$_6$) δ (ppm): 0.83 and 0.99 (2d, J = 6.8 and 6.8 Hz, 12H, 4 × CH_3), 2.57 (t, J = 5.9 Hz, 2H, CH_2CN), 3.35–3.40 (m, 2H, 2 × NCH), 3.45–3.51 (m, 2H, NCCH$_2$C*H*$_2$OP), 3.90–4.01 (m, 2H, CH$_2$C*H*$_2$OP), 4.62 (t, J = 5.7 Hz, 2H, C*H*$_2$CH$_2$OP), 7.15 (dd, J = 5.1 Hz, J = 3.6 Hz, 1H, $H_{thio.}$), 7.19–7.24 (m, 1H, $H_{aro.}$), 7.43–7.53 (m, 3H, 1$H_{thio.}$ and 2$H_{aro.}$), 7.62–7.68 (m, 2H, 1$H_{thio.}$ and 1$H_{aro.}$), 7.74 (dd, J = 8.6 Hz, J = 1.8 Hz, 1H, $H_{aro.}$), 8.23 (d, J = 7.5 Hz, 1H, $H_{aro.}$), 8.44 (d, J = 1.6 Hz, 1H, $H_{aro.}$). ^{13}C NMR (DMSO-d$_6$) δ (ppm): 19.6 (*C*H_2CN), 24.2 (4 × CH_3), 42.2 (2 × NCH), 43.6 (*C*H_2CH$_2$OP), 58.0, 61.2 (CH$_2$*C*H$_2$OP and NCCH$_2$*C*H$_2$OP), 109.8 ($C_{aro.}$), 110.1 ($C_{aro.}$), 117.0 (CH$_2$*C*N), 118.7, 118.9, 120.4, 122.1, 122.2, 122.6, 123.6, 124.1, 125.0, 125.8, 128.3, 139.8, 140.7, 144.8 ($C_{aro.}$). ^{31}P NMR (DMSO-d$_6$) δ (ppm): 146.67. HRMS (ESI) m/z $[M + Na]^+$ calcd for $C_{27}H_{32}N_3NaO_2PS$: 516.1850, found: 516.1868.

Oligonucleotide synthesis, purification and analysis

Oligonucleotide synthesis was performed on a PerSeptive Biosystems expedite 8909 automated DNA/RNA synthesizer on a 1.0 μmol scale on polystyrene supports 40s (from Amersham Biosciences) for oligonucleotides **ON1–ON3**. The manufacturer's standard cycle protocol was carried out using 4,5-dicyanoimidazole as an activator for the commercial phosphoramidites. A solution of the synthesized carbazole phosphoramidite **5** was prepared in a 1 mL dry plastic syringe by addition of anhydrous 5-[3,5-bis(trifluoromethyl)phenyl]-1*H*-tetrazole (0.25 M, in anhydrous acetonitrile) as an activator, followed by incorporation *via* hand-coupling[57] into the growing oligonucleotide chain during an extended coupling time (25 min). Due to its high sensitivity to humidity and light, the carbazole phosphoramidite **5** was immediately used for DNA synthesis. The coupling time for the standard as well as LNA-T monomers was 144 s and stepwise coupling efficiencies, determined by the absorbance of the liberated trityl cation at 495 nm on a UV-VIS spectrophotometer, were >98% for standard DNA monomers and >99% for LNA-T monomer. Removal of nucleobase protecting groups and cleavage from the solid polystyrene supports for **ON1–ON3** were performed under standard conditions (1 ml of 32% aqueous ammonia, 12 h at 55 °C). Purification of the resulting oligonucleotides **ON1–ON3** was accomplished by DMT-ON reverse-phase HPLC (RP-HPLC) using the Waters system 600 equipped with a Waters XBridge OBD C18-column (19 × 1000 mm, 5 μm + precolumn: XBridge 10 × 10 mm, 5 μm, temperature column oven: 50 °C). Elution was performed starting with an isocratic hold of buffer A for 2 min followed by a linear gradient to 70% buffer B over 17 min at a flow rate of 5 mL min^{-1} (Buffer A: 0.05 M triethylammonium acetate in Milli-Q water, pH 7.4; Buffer B: 75% CH_3CN/25% Buffer A). The corresponding fractions with oligonucleotides were evaporated under a flow of nitrogen, and oligonucleotides **ON1** and **ON2** were detritylated using an 80% aqueous solution of acetic acid (100 μL) for 30 min. Desalting was performed by addition of an aqueous solution of sodium acetate (3 M, 15 μL) and sodium perchlorate (5 M, 15 μL) and precipitation from cold acetone (1 mL). **ON3** was treated with 100 μL doubly filtered water followed by the addition of sodium perchlorate (5 M, 15 μL) before precipitation from cold acetone (1 mL). The resulting suspension for all oligonucleotides **ON1–ON3** was stored at −20 °C for 1 h. After centrifugation (13 000 rpm,10 min, 4 °C), the supernatant was removed and the pellet was further washed with cold acetone (2 × 1 mL), dried for 30 min under a flow of nitrogen, and dissolved in Milli-Q water (1 ml).

Table 4 MALDI-MS and the HPLC purity of the synthesized ONs

ON#	Sequence	Calc. *m/z*	Found *m/z*	HPLC purity
ON1	5′-GTG ATA TGC-3′	2753.84	2749.76	94%
ON2	5′-GTG AT^{L}A TGC-3′	2781.84	2779.23	96%
ON3	5′-ZGTG AT^{L}A TGC-3′	3138.19	3136.01	93%

The composition of the oligonucleotides (Table 4) was confirmed by MALDI-TOF analysis on a Bruker Daltonics Microflex *LT* (MALDI-LIFT system) MS instrument in the ES^{+} mode.

The purity for all final oligonucleotides **ON1–ON3** was found to be more than 93% when recorded using analytical IE-HPLC traces using a Merck Hitachi La-Chrom system equipped with a DNAPac PA100, analytical column (13 μm, 250 mm × 4 mm) heated to 60 °C. Elution was performed with an isocratic hold of buffer (10%), starting from 2 min hold on 2% Eluent in Milli-Q water (solvent A), followed by a linear gradient to 30% eluent in 23 min at a flow rate of 1.1 mL min^{-1} (eluent: 0.6 M sodium perchlorate; buffer: 0.25 M Tris-Cl, pH 8.0; solvent A: Milli-Q water).

UV thermal melting studies

In order to determine duplex melting temperatures (T_m), UV melting measurements were performed on a PerkinElmer Lambda 35 UV-Vis spectrometer fitted with a PTP-6 Peltier temperature programmer using Hellma SUPRASIL synthetic quartz optical cuvettes with a path length of 10 mm. Concentrations of purified oligonucleotides were determined by UV analysis at 260 nm, assuming identical molar absorptivities for unmodified DNA, RNA and LNA nucleoside constituents (ε_{260}: dG = 10.8, dT = 8.4, dA = 13.7, dC = 7.3, rG = 10.8, rU = 9.8, rA = 13.7, rC = 7.1, T^{L} = 8.4 OD$_{260}$ μmol^{-1}). The extinction coefficient[58] was determined for the thiophenyl carbazole moiety (ε_{260} = 19.71 OD$_{260}$ μmol^{-1}) after measuring the absorbance average of three measurements for **Z** linker. The synthesized oligonucleotides **ON1–ON3** (2.5 μM) were mixed with a complementary DNA/RNA strand concentration of 2.5 μM and a volume of 1.0 mL before monitoring at 260 nm. Samples were prepared as follows: the two strands were mixed in a 1 : 1 ratio in 2 mL Eppendorf tubes before medium salt buffer (2 times, 11.7 mM sodium phosphate, 200 mM NaCl, 0.20 mM EDTA, pH 7.0, 500 μL) was added, which was completed in 1.0 mL using Milli-Q water. Thus, all oligonucleotide samples were dissolved under 1× buffer conditions (5.8 mM sodium phosphate, 100 mM NaCl and 0.10 mM EDTA) to furnish duplex-forming oligonucleotides. The samples were denatured by heating to 90 °C (10 min) in a water bath followed by gradually cooling to the starting temperature of the experiment of 8 °C and were then kept at this temperature for 120 min before they were transferred into the cuvettes. The thermal melting temperatures (T_m, °C) were determined as the maximum of the first derivative plots of the smoothed melting curves obtained from the UV absorbance at 260 nm (as a function of time) against the increasing temperature from 8 °C to 70 °C (gradient 0.5 °C min^{-1}) programmed using a Peltier temperature controller. All melting temperatures are within the uncertainty ± 0.5 °C as determined by repetitive experiments and T_m values were calculated using UV-WinLab software, taking an average of the two separate melting curves. ΔT_m values were calculated as the difference in T_m values between the unmodified and modified duplexes. For mismatched duplexes, ΔT_m values were calculated as the difference in T_m values between the mismatched and matched duplexes. Due to unclear transition for the mismatched duplex melting curve for **ON1**/**R5** using a medium salt buffer, UV melting measurements were repetitively recorded at pH 7.0 under high salt buffer conditions (5.1 mM sodium phosphate, containing 1 M NaCl and 0.10 mM EDTA) for **ON1**/(**R1**, **R5**, **R6**, **R7**).

Circular dichroism studies

CD measurements were performed on a Jasco J-815 spectropolarimeter using 1 mL quartz cuvettes with 5 mm path length. Oligonucleotides (2.5 μM) were mixed in a medium salt buffer (5.8 mM NaH_2PO_4/Na_2HPO_4, containing 100 mM NaCl and 0.10 mM EDTA) at pH 7.0 using the same solution used for T_m measurements. All samples were annealed for 2 min at 90 °C and slowly cooled to room temperature before data collection. The measurements were performed at 20 °C in the 200–400 nm wavelength range with a continuous scanning mode, 50 nm min^{-1} as a scanning speed, 4 s for a response, 2.0 nm for bandwidth. In order to confirm the very low thermal melting value for the mismatched duplex **ON1**/**R5**, CD spectra were recorded at pH 7.0 under high salt buffer conditions (5.1 mM sodium phosphate, containing 1 M NaCl and 0.10 mM EDTA) for the mismatched duplexes **ON1**/(**R1**, **R5**, **R6**, **R7**) in addition to measurements using a medium salt buffer. All CD profiles were attained by taking the average of five accumulations from which the spectrum of the background buffer was subtracted. The spectra were smoothened in Microcal Origin 6.0 using a Savitzky–Golay filter.

UV absorption spectra

UV-vis absorption spectra (range: 200–600 nm) were recorded at 20 °C using the same samples and instrumentation as in the thermal denaturation experiments.

Steady-state fluorescence emission spectra

Fluorescence spectra (350–600 nm) of ONs modified with carbazole-functionalized monomer **Z** and the corresponding matched and mismatched duplexes with complementary DNA/DNA and DNA/RNA targets were recorded with a Varian-Cary Eclipse spectrophotometer using quartz Suprasil cuvettes with a path length of 10.00 mm. The fluorescence experiments were conducted at 20 °C in non-deoxygenated thermal denaturation buffer (5.8 mM NaH_2PO_4/Na_2HPO_4, containing 100 mM NaCl and 0.10 mM EDTA at pH 7.0, each strand at 2.5 μM concentration) and obtained as an average of five scans with the use of an excitation wavelength of 310 nm, an excitation slit of 5.0 nm, an emission slit of 5.0 nm and a scan speed of 600 nm min^{-1} with a medium scanning mode using medium voltage.

The samples from the thermal denaturation experiments were reused for the fluorescence measurements. All samples were annealed at 90 °C for 10 min and allowed to cool slowly to room temperature prior to measurements. Background spectra of buffer solution were recorded with an excitation wavelength of 310 nm and were subtracted from the relevant spectra.

Molecular modelling

Molecular modelling was performed with Maestro v9.2 from Schrödinger. All calculations were conducted with AMBER* force field[59] and the implicit GB/SA water model[60] as implemented in MacroModel v9.2. Extended cut-offs were used for non-bonded interactions (van der Waals 8 Å and electrostatics 20 Å). The molecular dynamic simulations were performed with stochastic dynamics, a SHAKE algorithm to constrain bonds to H-atoms, a time step of 1.5 fs, and a simulation temperature of 300 K. Simulation for 0.5 ns with an equilibration time of 150 ps generated 250 individual structures, which were minimized using the Polak–Ribiere Conjugate Gradient (PRCG) method[61] with the maximum iterations of 5000 and the convergence threshold of 0.05 kJ mol^{-1}. The resulting structures were compared in order to determine the lowest-energy conformers. The global minimum was used for analysis. For the **Z**-modified DNA/DNA duplex **ON3**/**D1**, the starting structure was generated by building a standard B-type DNA duplex conformation using MacroModel v9.2, followed by: (i) modifying with the LNA-T monomer together with terminal incorporation of the desired carbazole monomer **Z** at the DNA 9-mer strand **ON3**, (ii) terminal insertions of two 3-mer overhangs (**CTT**, **CTC**) at the 3′- and 5′-opposing ends of the complementary DNA stand **D1**, respectively.

For the **Z**-modified DNA/RNA duplex **ON3**/**R1**, the seed structure was generated by taking the previously reported NMR solution structure of the LNA : RNA hybrid duplex obtained from the Protein Data Bank (PDB ID: 1HHW).[54] For the wrong number of bonds and missing hydrogens observed in the best representative conformer of the NMR ensemble, manual fixing was carried out using the Build panel for bonds and Add hydrogens preprocessing step for missing hydrogens, while observed hydrogen overlaps were fixed *via* optimizing H-bond assignment. For precise positioning and accurate model calculations, the cytosine attached at the 5′-end of **ON3** was modified by guanine, whereas the guanine at the 3′-opposing end of **R1** was adjusted by cytosine in order to build a corrected base pair which fully matched with the tested DNA/RNA duplex construct. The model of the modified **ON3**/**R1** duplex was performed by incorporation of the carbazole monomer **Z** at the 5′-end of **ON3**, followed by incorporations of the two 3-mer overhangs (**CUU**, **CUC**) at the 3′- and 5′-opposing ends of the complementary RNA stand **R1**, respectively.

Initially, all atoms except for those in the carbazole monomer **Z** and LNA-T were frozen to perform a relaxation of the modified nucleotide, and then a complete minimization of the full duplexes (**ON3**/**D1**, **ON3**/**R1**) was carried out to attain a relaxed low-energy duplex before applying dynamic simulations described above. Hundreds of conformations were found for carbazole-modified DNA/DNA (**ON3**/**D1**) as well as DNA/RNA (**ON3**/**R1**) duplex structures within the energy window. The resulting structures were further processed in VMD (v1.9.3a6, 2015. http://www.ks.uiuc.edu) or in PyMOL (v1.7.4.5, 2010. http://pymol.org) Molecular Graphics Systems.

Conflicts of interest

The authors declare no conflict of interest.

Acknowledgements

This work was financially supported by the Biomolecular Nanoscale Engineering Center of Excellence (BioNEC) funded by the VILLUM FONDEN for studies on nucleic acid chemical biology, Grant Number VKR18333, from the European Union's Horizon 2020 research and innovation program under grant agreement no 810685, and from the Silesian University of Technology BKM-RCh-2020.

Notes and references

1 G. F. Deleavey and M. J. Damha, *Chem. Biol.*, 2012, **19**, 937–954.
2 C. Chen, Z. Yang and X. Tang, *Med. Res. Rev.*, 2018, **38**, 829–869.
3 T. R. Gingeras, R. Higuchi, L. J. Kricka, Y. M. D. Lo and C. T. Wittwer, *Clin. Chem.*, 2005, **51**, 661–671.
4 J. D. Watson, A. A. Caudy, R. M. Myers and J. A. Witkowski, *Recombinant DNA: Genes and Genomes-A Short Course*, 3rd edn, W.H. Freeman, New York, NY, 2007.
5 (*a*) Y. Fichou and C. Ferec, *Trends Biotechnol.*, 2006, **24**, 563–570; (*b*) Y. Singh, P. Murat and E. Defrancq, *Chem. Soc. Rev.*, 2010, **39**, 2054–2070; (*c*) J. Wengel, *Org. Biomol. Chem.*, 2004, **2**, 277–280; (*d*) J. Bath and A. J. Turberfield, *Nat. Nanotechnol.*, 2007, **2**, 275–284; (*e*) N. C. Seeman, *Annu. Rev. Biochem.*, 2010, **79**, 65–87; (*f*) O. I. Wilner and I. Willner, *Chem. Rev.*, 2012, **112**, 2528–2556.
6 (*a*) W. B. Wan and P. P. Seth, *J. Med. Chem.*, 2016, **59**, 9645–9667; (*b*) T. Habuchi, T. Yamaguchi, H. Aoyama, M. Horiba, K. R. Ito and S. Obika, *J. Org. Chem.*, 2019, **84**, 1430–1439.
7 J. Wengel, *Acc. Chem. Res.*, 1999, **32**, 301–310.
8 N. M. Bell and J. Micklefield, *ChemBioChem*, 2009, **10**, 2691–2703.
9 T. Yamamoto, M. Nakatani, K. Narukawa and S. Obika, *Future Med. Chem.*, 2011, **3**, 339–365.
10 K. R. Fox and T. Brown, *Biochem. Soc. Trans.*, 2011, **39**, 629–634.
11 G. F. Deleavey and M. J. Damha, *Chem. Biol.*, 2012, **19**, 937–954.
12 M. A. Campbell and J. Wengel, *Chem. Soc. Rev.*, 2011, **40**, 5680–5689.
13 S. Obika, S. M. A. Rahman, A. Fujisaka, Y. Kawada, T. Baba and T. Imanishi, *Heterocycles*, 2010, **81**, 1347–1392.

14 K. E. Lundin, T. Højland, B. R. Hansen, R. Persson, J. B. Bramsen, J. Kjems, T. Koch, J. Wengel and C. I. E. Smith, *Adv. Genet.*, 2013, **82**, 47–107.
15 (*a*) S. Tyagi and F. R. Kramer, *Nat. Biotechnol.*, 1996, **14**, 303–308; (*b*) T. Heyduk and E. Heyduk, *Nat. Biotechnol.*, 2002, **20**, 171–176; (*c*) M. K. Johansson and R. M. Cook, *Chem. – Eur. J.*, 2003, **9**, 3466–3471; (*d*) W. Tan, K. Wang and T. J. Drake, *Curr. Opin. Chem. Biol.*, 2004, **8**, 547–553.
16 (*a*) K. Nakatani, *ChemBioChem*, 2004, **5**, 1623–1633; (*b*) R. T. Ranasinghe and T. Brown, *Chem. Commun.*, 2005, 5487–5502; (*c*) M. Strerath and A. Marx, *Angew. Chem., Int. Ed.*, 2005, **44**, 7842–7849.
17 (*a*) O. Köhler, D. V. Jarikote and O. Seitz, *ChemBioChem*, 2005, **6**, 69–77; (*b*) D. V. Jarikote, N. Krebs, S. Tannert, B. Röder and O. Seitz, *Chem. – Eur. J.*, 2007, **13**, 300–310; (*c*) E. Socher, D. V. Jarikote, A. Knoll, L. Röglin, J. Burmeister and O. Seitz, *Anal. Biochem.*, 2008, **375**, 318–330.
18 A. Okamoto, K. Tainaka, Y. Ochi, K. Kanatani and I. Saito, *Mol. Biosyst.*, 2006, **2**, 122–127.
19 B. Venkatesan, Y. J. Seo and B. H. Kim, *Chem. Soc. Rev.*, 2008, **37**, 648–663.
20 (*a*) A. S. Boutorine, D. S. Novopashina, O. A. Krasheninina, K. Nozeret and A. G. Venyaminova, *Molecules*, 2013, **18**, 15357–15397; (*b*) A. Okamoto, Y. Saito and I. Saito, *J. Photochem. Photobiol., C*, 2005, **6**, 108–122; (*c*) K. M. Wang, Z. W. Tang, C. Y. J. Yang, Y. M. Kim, X. H. Fang, W. Li, Y. R. Wu, C. D. Medley, Z. H. Cao, J. Li, P. Colon, H. Lin and W. H. Tan, *Angew. Chem., Int. Ed.*, 2009, **48**, 856–870; (*d*) U. Asseline, *Curr. Org. Chem.*, 2006, **10**, 491–518.
21 V. V. Filichev, M. C. Nielsen, N. Bomholt, C. H. Jessen and E. B. Pedersen, *Angew. Chem., Int. Ed.*, 2006, **45**, 5311–5315.
22 F. Lewis, L. G. Zhang and X. B. Zuo, *J. Am. Chem. Soc.*, 2005, **127**, 10002–10003.
23 S. M. Langenegger and R. Häner, *ChemBioChem*, 2005, **6**, 848–851.
24 M. Nakamura, Y. Fukunaga, K. Sasa, Y. Ohtoshi, K. Kanaori, H. Hayashi, H. Nakano and K. Yamana, *Nucleic Acids Res.*, 2005, **33**, 5887–5895.
25 K. Yamana, T. Gokota, H. Ozaki, H. Nakono, O. Sangen and T. Shimidzu, *Nucleosides Nucleotides*, 1992, **11**, 383–390.
26 D. Honcharenko, C. Zhou and J. Chattopadhyaya, *J. Org. Chem.*, 2008, **73**, 2829–2842.
27 C. Dohno and I. Saito, *ChemBioChem*, 2005, **6**, 1075–1081.
28 K. V. Balakin, V. A. Korshun, I. I. Mikhalev, G. V. Maleev, A. D. Malakhov, I. A. Prokhorenko and Y. A. Berlin, *Biosens. Bioelectron.*, 1998, **13**, 771–778.
29 D. Lindegaard, A. S. Madsen, I. V. Astakhova, A. D. Malakhov, B. R. Babu, V. A. Korshun and J. Wengel, *Bioorg. Med. Chem.*, 2008, **16**, 94–99.
30 V. L. Malinovskii, D. Wenger and R. Häner, *Chem. Soc. Rev.*, 2010, **39**, 410–422.
31 M. E. Østergaard and P. J. Hrdlicka, *Chem. Soc. Rev.*, 2011, **40**, 5771–5788.
32 P. Perlíkov, M. Ejlersen, N. Langkjær and J. Wengel, *ChemMedChem*, 2014, **9**, 2120–2127.
33 I. V. Astakhova, V. A. Korshun, K. Jahn, J. Kjems and J. Wengel, *Bioconjugate Chem.*, 2008, **19**, 1995–2007.
34 C. B. Nielsen, M. Petersen, E. B. Pedersen, P. E. Hansen and U. B. Christensen, *Bioconjugate Chem.*, 2004, **15**, 260–269.
35 A. Głuszyńska, *Eur. J. Med. Chem.*, 2015, **94**, 405–426.
36 A. Głuszyńska, B. Juskowiak, M. Kuta-Siejkowska, M. Hoffmann and S. Haider, *Int. J. Biol. Macromol.*, 2018, **114**, 479–490.
37 A. Głuszyńska, B. Juskowiak, M. Kuta-Siejkowska, M. Hoffmann and S. Haider, *Molecules*, 2018, **23**, 1134.
38 M. D. Matteucci and U. V. Krosigk, *Tetrahedron Lett.*, 1996, **37**, 5057–5060.
39 T. Sakamoto, Y. Tanaka and K. Fujimoto, *Org. Lett.*, 2015, **17**, 936–939.
40 K. Fujimoto, K. Hiratsuka-Konishi, T. Sakamoto, T. Ohtake, K. Shinohara and Y. Yoshimura, *Mol. BioSyst.*, 2012, **8**, 491–494.
41 S. K. Singh, R. Kumar and J. Wengel, *J. Org. Chem.*, 1998, **63**, 10035–10039.
42 K. Fluiter, M. Frieden, J. Vreijling, C. Rosenbohm, M. B. De Wissel, S. M. Christensen, T. Koch, H. Ørum and F. Baas, *ChemBioChem*, 2005, **6**, 1104–1109.
43 R. Owczarzy, Y. You, C. L. Groth and A. V. Tataurov, *Biochemistry*, 2011, **50**, 9352–9367.
44 A. S. Jørgensen, L. H. Hansen, B. Vester and J. Wengel, *Bioorg. Med. Chem. Lett.*, 2014, **24**, 2273–2277.
45 I. K. Astakhova and J. Wengel, *Acc. Chem. Res.*, 2014, **47**, 1768–1777.
46 L. Przypis and K. Z. Walczak, *J. Org. Chem.*, 2019, **84**, 2287–2296.
47 M. S. Ho, C. Barrett, J. Paterson, M. Esteghamatian, A. Natansohn and P. Rochon, *Macromolecules*, 1996, **29**, 4613–4618.
48 A. A. Koshkin, S. K. Singh, P. Nielsen, V. K. Rajwanshi, R. Kumar, M. Meldgaard, C. E. Olsen and J. Wengel, *Tetrahedron*, 1998, **54**, 3607–3630.
49 V. V. Filichev and E. B. Pedersen, *J. Am. Chem. Soc.*, 2005, **127**, 14849–14858.
50 A. M. A. Osman, P. T. Jørgensen, N. Bomholt and E. B. Pedersen, *Bioorg. Med. Chem.*, 2008, **16**, 9937–9947.
51 U. B. Christensen and E. B. Pedersen, *Nucleic Acids Res.*, 2002, **30**, 4918–4925.
52 K. M. Guckian, B. A. Schweitzer, R. X.-F. Ren, C. J. Sheils, P. L. Paris, D. C. Tahmassebi and E. T. Kool, *J. Am. Chem. Soc.*, 1996, **118**, 8182–8183.
53 (*a*) V. V. Filichev and E. B. Pedersen, *Org. Biomol. Chem.*, 2003, **1**, 100–103; (*b*) V. V. Filichev, K. M. H. Hilmy, U. B. Christensen and E. B. Pedersen, *Tetrahedron Lett.*, 2004, **45**, 4907–4910; (*c*) A. M. A. Osman and E. B. Pedersen, *Monatsh. Chem.*, 2010, **141**, 817–822; (*d*) P. Perlíkov, K. K. Karlsen, E. B. Pedersen and J. Wengel, *ChemBioChem*, 2014, **15**, 146–156.
54 M. Petersen, K. Bondensgaard, J. Wengel and J. P. Jacobsen, *J. Am. Chem. Soc.*, 2002, **124**, 5974–5982.
55 J. M. Chalker, A. L. Thompson and B. G. Davis, *Org. Synth.*, 2010, **87**, 288–302.

56 S. H. Tucker, *J. Chem. Soc., Dalton Trans.*, 1924, **125**, 1144–1148.
57 L. Kværnø, R. Kumar, B. M. Dahl, C. E. Olsen and J. Wengel, *J. Org. Chem.*, 2000, **65**, 5167–5176.
58 M. J. Cavaluzzi and P. N. Borer, *Nucleic Acids Res.*, 2004, **32**, e13.
59 (*a*) S. J. Weiner, P. A. Kollman, D. A. Case, U. C. Singh, C. Ghio, G. Alagona, S. Profeta and P. Weiner, *J. Am. Chem. Soc.*, 1984, **106**, 765–784; (*b*) S. J. Weiner, P. A. Kollman, D. T. Nyguyen and D. A. Case, *J. Comput. Chem.*, 1986, **7**, 230–252.
60 W. C. Still, A. Tempczyk, R. C. Hawlay and T. Hendrickson, *J. Am. Chem. Soc.*, 1990, **112**, 6127–6129.
61 E. Polak and G. Ribière, *Revue Francaise Ḋinformat et de Recherche Opérationelle*, 1969, **16**, 35–43.